IEEJ Journal of Industry Applications
Vol.8 No.3 pp.430–436 DOI: 10.1541/ieejjia.8.430

Paper

Reduction of Torque Ripple in Synchronous Reluctance Motor by Combining Different Flux Barrier Structures

Yuuto Yamamoto* Student Member, Shigeo Morimoto*a) Senior Member
Masayuki Sanada* Senior Member, Yukinori Inoue* Member

(Manuscript received June 20, 2018, revised Oct. 26, 2018)

A synchronous reluctance motor (SynRM) is an inexpensive variable-speed motor that is receiving increased attention as a rare-earth-free motor. However, a concern regarding such motors is them having a high torque ripple, which generates undesirable noise and vibration. The focus of this study is to minimize the torque ripple of a SynRM by combining different flux barrier structures in the rotor. The effects of various flux barrier configurations on the motor's torque performance were examined, and two different flux barrier structures were combined by lamination in an asymmetric rotor structure. Further, the rotor was constructed by stacking two different rotor laminations with different flux barrier structures. The torque performance of the proposed SynRMs was evaluated using the two-dimensional finite element method.

Keywords: synchronous reluctance motor, rare-earth-free motor, torque ripple reduction, asymmetric flux barriers

1. Introduction

Currently, permanent magnet synchronous motors (PMSMs) with rare-earth permanent magnets are used for various applications because of their high efficiency and wide range of operating speed [1]. However, rare-earth materials are expensive and can be produced in specific areas. Therefore, it is necessary to reduce the use of rare-earth materials [2][3]. To replace PMSMs using rare-earth elements, synchronous reluctance motors (SynRMs) are receiving increased attention as rare-earth-free motors [4]–[9]. SynRMs have also attracted attention as a high efficiency motor for industrial use, and SynRMs that meet Premium/IE3 and Super-Premium/IE4 efficiency class have been developed [10].

In general, SynRMs are inexpensive variable-speed motors because they consist of only the core and winding. However, the disuse of permanent magnets causes the torque and efficiency of SynRMs to be inferior to those of PMSMs. In addition, SynRMs, which utilize reluctance torque, have the disadvantage of having a higher torque ripple. Thus, a suitable structure that achieves a large average torque and the low torque ripple should be examined [11]–[15]. In Ref. (11), it is shown that the reduction of torque ripple can be achieved by means of a suitable choice of the number of flux barrier with respect to the number of stator slots based on permeance model. An asymmetric flux barrier arrangement was proposed in Ref. (14), where the relative position between all the flux barriers and stator teeth are uniformly distributed base on the slot pitch and number of poles. Then the asymmetric flux barrier arrangement was applied to the SynRM and IPMSM with two flux barriers per pole, and the torque characteristics were evaluated. The rotor formed by two different lamination was proposed in Ref. (13). This strategy combines a suitable choice of the position of the flux barrier ends with the adaption of two different rotor laminations. This strategy was applied to the SynRMs with one flux barrier per pole and two flux barriers per pole, and the torque characteristics were evaluated. In Ref. (14), an asymmetric flux barrier arrangement, in which two different flux-barrier geometries are adapted in the same lamination, was proposed in addition to the strategy formed the rotor with laminations of two different kinds. This structure was applied to the SynRM and PMASynRM with two flux barriers per pole. Although the forgoing methods were applied to SynRMs having a relatively small number of flux barriers (one or two), and the torque characteristics were evaluated, the multi flux barrier structure (four or more barriers per pole) common as SynRM had not been verified. An asymmetric flux barrier arrangement is also proposed for a SynRM with four flux-barriers per pole in Ref. (15). The barrier construction and barrier tip construction were designed by using a optimization software package with FE package, but the process of rotor design was a black box and the reason why the torque ripple can be reduced was unclear.

This study investigated how to reduce the torque ripple without also reducing the average torque combining different flux barrier structures in a six-flux-barrier SynRM having a relatively large number of flux barriers [16]. The proposed design process for reducing torque ripple is systematic and simple.

First, in order to simplify the design process, one design parameter of the magnetic flux barrier angle was varied to investigate the influence of change in the flux barrier angle on the torque characteristics. Next, the torque characteristics of

a) Correspondence to: Shigeo Morimoto. E-mail: morimoto@eis.osakafu-u.ac.jp
* Osaka Prefecture University
1-1, Gakuencho, Naka-ku, Sakai, Osaka 599-8531, Japan

Table 1. Common specifications of analysis models and analytical conditions

Item (Unit)	Value
Number of turns per slot	16
Stator outer diameter (mm)	204
Stator inner diameter (mm)	127
Rotor outer diameter (mm)	126
Rotor inner diameter (mm)	48
Air gap length (mm)	0.5
Stack length (mm)	90
Winding resistance (20°C) (Ω)	0.268
Magnetic steel sheet	50H470
Rated phase current (A)	16.4
Rotational speed (min^{-1})	3000

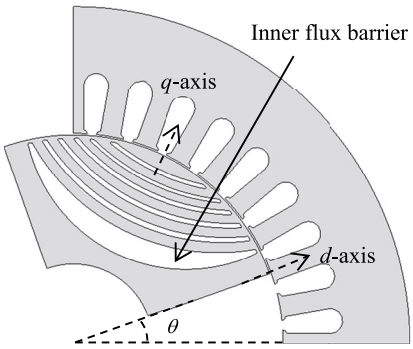

Fig. 1. Structure of reference model (Type-R)

the SynRM when combining two kinds of flux barrier shapes with different flux barrier angles were investigated. As a result, an optimal combination of two kinds of flux barrier shapes that minimizes the torque ripple was found. In these investigations, the influence of the flux barrier angle on the phase as well as the amplitude of the harmonic components of instantaneous torque waveform was also analyzed and discussed. An asymmetric rotor structure, in which two different flux barrier geometries are adapted in the same lamination, was proposed, and its torque performance was analyzed by the two-dimensional finite element method (FEM). Moreover, the rotor formed by stacking two different rotor laminations with different flux barrier angle was proposed. We investigated the relationship between the ratio of stack length of two different rotor laminations and the torque ripple, and found the optimum ratio. Finally, we compared the characteristics of the proposed SynRM optimally designed to reduce torque ripple and the reference SynRM, and confirmed that the proposed SynRM can reduce torque ripple by about half with almost no decrease in average torque.

2. Characteristics of Reference Model

Table 1 shows the common specifications of the analysis models and analytical conditions in this study. Figure 1 shows the structure of the reference model (Type-R), where θ is rotor position indicated by spacial mechanical angle. The stator is same as a stator for 7.5 kW industrial induction motor and has 4 poles and a distributed winding with 36 slots. The reference model was properly designed based on the design guidelines shown in references [4][5][7]. The rotor of the reference model has 6 flux barriers, where the ratio of the slit width to the rib width is 2:1. The wide inner flux barrier of

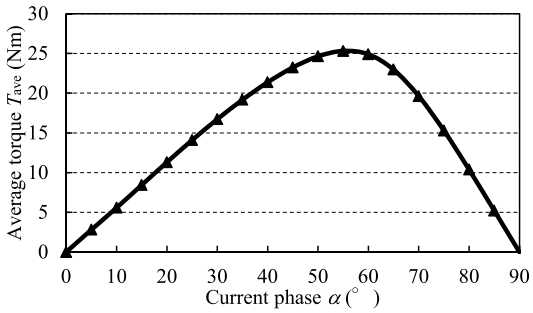

Fig. 2. Average torque versus current phase characteristics of Type-R (I_e = 16.4 A)

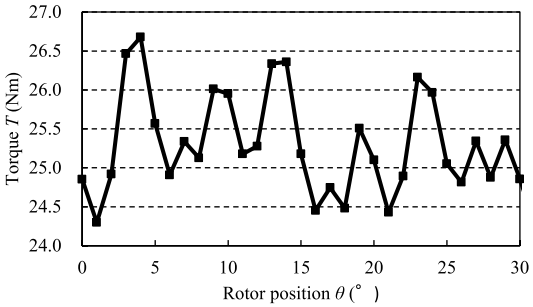

Fig. 3. Instantaneous torque versus rotor position angle in Type-R (I_e = 16.4 A)

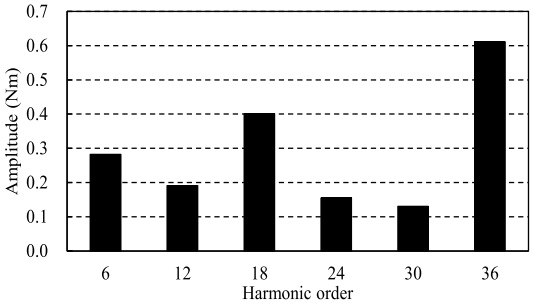

Fig. 4. Amplitude of harmonic components of instantaneous torque waveform for Type-R

Type-R was intended to reduce the q-axis inductance. In the analysis of this paper, a two-dimensional (2D) finite element analysis by JMAG-Designer was basically used.

Figure 2 shows the average torque versus the current phase, where the phase current I_e was 16.4 A. The current phase α which is time domain phase angle represents the leading angle of the current vector from the d-axis. As shown in Fig. 2, the maximum torque for Type-R is 25.31 Nm when $\alpha = 55°$.

Figure 3 shows the instantaneous torque versus the rotor position angle when I_e = 16.4 A and $\alpha = 55°$. Here, θ is the geometrical rotor position angle as shown in Fig. 1. The torque ripple ratio *TRR* is defined by

$$TRR = \frac{\Delta T}{T_{\text{ave}}} = \frac{T_{\max} - T_{\min}}{T_{\text{ave}}} \times 100(\%) \cdots\cdots\cdots\cdots (1)$$

where ΔT is the difference between the maximum torque $T_{\max}$ and the minimum torque $T_{\min}$, and T_{ave} is the average torque. As shown in Fig. 3, $T_{\max}$ is 26.7 Nm and $T_{\min}$ is 24.3 Nm; thus, the torque ripple ratio *TRR* for Type-R is 9.52%.

Figure 4 shows the harmonic components of the instantaneous torque waveform. As can be seen, torque ripple occurs

approximately at multiples of 6, and in particular, the 6th, 18th, and 36th harmonic components are large. This is attributed to the positional relationship between the slots of the stator and the flux barriers of the rotor.

3. Effect of Flux Barrier Angle on Torque Characteristics

Figure 5 shows the analytical rotor structure. In this model, the centers of flux barriers are fixed and the edges of all six flux barriers are shifted by δ (°) which is a spacial mechanical angle in a tangential direction with respect to the barrier position of the reference model (Type-R); we refer to this model as Type-Rδ.

Figure 6 shows the average torque and torque ripple versus shift angle of the flux barrier. The average torque is almost constant over the entire δ region. However, the torque ripple ratio changes depending on δ. It has a minimum value of 9.52% when δ is 0°. It can be seen that the flux barrier angle of the reference model (Type-R) in which $\delta = 0°$ is optimally designed so as to minimize the torque ripple.

Figure 7 shows the amplitude of the harmonic components of instantaneous torque versus the flux barrier angle. The amplitude of the 6th harmonic component is relatively small and is almost constant over the entire δ region. However, the changes in amplitudes of the 18th and 36th harmonic components are large.

Figure 8 shows the phase of the harmonic components versus the angle of the flux barrier. The phase of the 6th harmonic component is almost constant over the entire δ region. However, the phase of the 18th harmonic component increases monotonically, and the phase of the 36th harmonic component changes sharply between $\delta = -2.5°$ and $\delta = -2.0°$ and between $\delta = 0°$ and $\delta = 0.5°$.

These results confirmed that the flux barrier angle influences the torque ripple and the amplitude and phase of the harmonic components, especially the 18th and 36th harmonic components. The other harmonic components such as 12th and 24th were also analyzed, and it was confirmed that the amplitudes of other harmonic components are almost constant regardless of δ.

4. Model Combining Rotors with Different Flux Barrier Angles

The results in section 3 suggest that the torque ripple can be reduced by combining different flux barrier structures so as to cancel the harmonic components of instantaneous torque.

In this section, SynRM with rotor structure formed by combining two flux barrier designs with different flux barrier angles δ_1 and δ_2 ($\delta_1 \le \delta_2$), which is indicated as Type-R$\delta_1\delta_2$, is investigated. The torque characteristics of Type-R$\delta_1\delta_2$ are calculated simply by averaging the instantaneous torques for Type-Rδ_1 and Type-Rδ_2.

Figure 9 shows the torque ripple ratio map for Type-R$\delta_1\delta_2$ when I_e is 16.4 A and α is 55°. The step size for the flux barrier angle is 0.5°. The model with the lowest torque ripple ratio in Fig. 9 was Type-R-1.5+1.5, with a torque ripple ratio of 6.2%.

As shown in Fig. 9, the torque ripple for a combination of $\delta_1 = -2.0 \sim -1.0°$ and $\delta_2 = 1.0 \sim 2.0°$ is especially low. Hence, the step size for the flux barrier angles was finely adjusted to 0.1° between $\delta_1 = -2.0 \sim -1.0°$ and $\delta_2 = 1.0 \sim 2.0°$. Figure 10 shows the torque ripple ratio map after adjusting the step size of flux barrier angle to 0.1°. The model with the lowest torque ripple ratio is Type-R-1.7+1.6, with a torque ripple ratio of 5.0%, which is 20.1% lower than

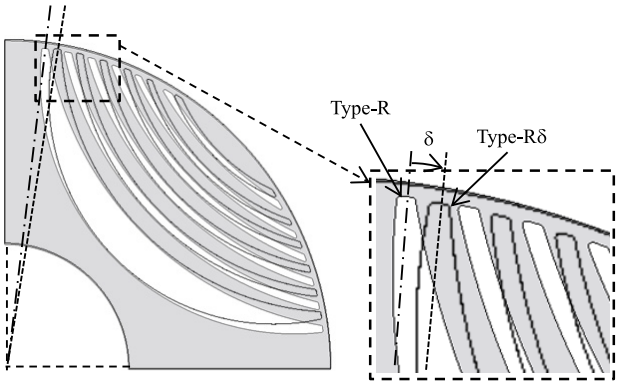

Fig. 5. Rotor model (Type-Rδ)

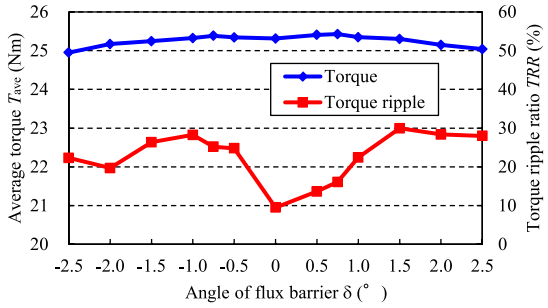

Fig. 6. Average torque and torque ripple versus flux barrier angle (I_e = 16.4 A, α = 55°)

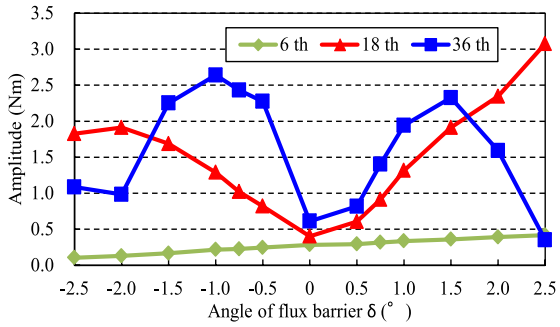

Fig. 7. Amplitude of harmonic components of instantaneous torque waveform for Type-Rδ (I_e = 16.4 A, α = 55°)

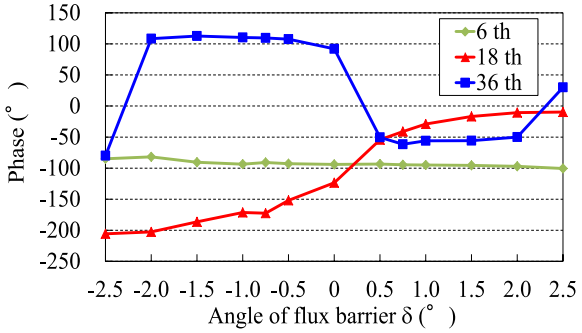

Fig. 8. Phase of harmonic components of instantaneous torque waveform for Type-Rδ (I_e = 16.4 A, α = 55°)

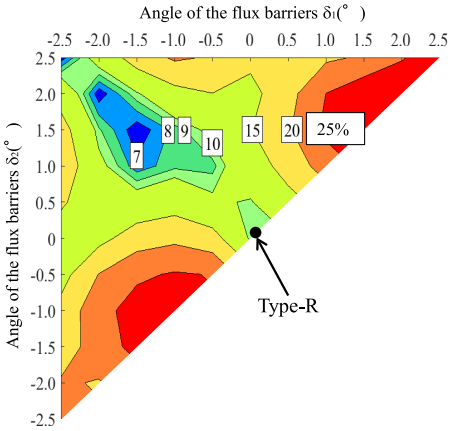

Fig. 9. Torque ripple ratio map for Type-R$\delta_1\delta_2$ with step size of 0.5° (I_e = 16.4 A, α = 55°)

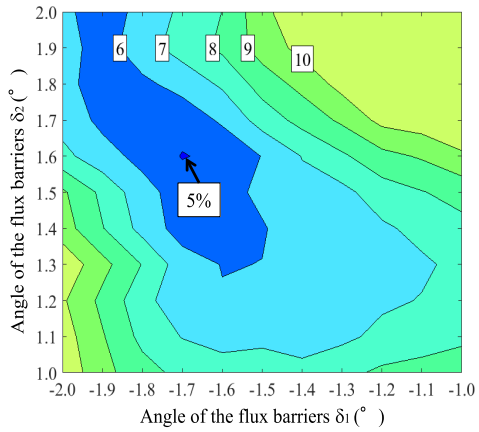

Fig. 10. Torque ripple ratio map for Type-R$\delta_1\delta_2$ with step size of 0.1° (I_e = 16.4 A, α = 55°)

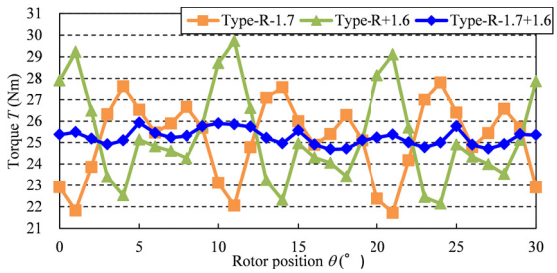

Fig. 11. Instantaneous torque vs. rotor position (I_e = 16.4 A, α = 55°)

that for Type-R-1.5+1.5.

Figure 11 shows the instantaneous torque versus rotor position for Type-R-1.7, Type-R+1.6, and Type-R-1.7+1.6. By combining Type-R-1.7 and Type-R+1.6, the instantaneous torque for each model could be canceled, and the torque ripple for Type-R-1.7+1.6 was reduced.

Table 2 shows that the amplitudes and the phases of the harmonic components for Type-R-1.7, Type-R+1.6, and Type-R-1.7+1.6, respectively. Comparing the 18th and 36th harmonic components, the amplitudes of Type-R-1.7 and Type-R+1.6 are almost equal, with a phase difference of approximately 180°. The torque ripple was reduced by canceling out of the 18th and 36th harmonic components of the instantaneous torques for Type-R-1.7 and Type-R+1.6.

Table 2. Amplitude and phase of harmonic components of instantaneous torque waveform

		Type-R -1.7	Type-R +1.6	Type-R -1.7+1.6
6th	Amplitude (N·m)	0.16	0.37	0.27
	Phase (°)	-89.09	-96.44	-94.33
18th	Amplitude (N·m)	1.70	1.97	0.15
	Phase (°)	169.33	-14.34	-35.76
36th	Amplitude (N·m)	1.73	1.94	0.30
	Phase (°)	113.20	-53.69	-13.10

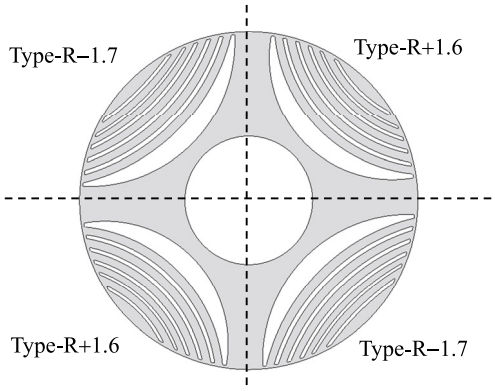

Fig. 12. Proposed asymmetric rotor structure for Type-ASR

Table 3. Torque characteristics at MTPA (I_e = 16.4 A)

Item (Unit)	Type-R-1.7+1.6	Type-ASR
α (°)	55	55
T_{ave} (N·m)	25.24	25.29
T_{max} (N·m)	25.93	26.08
T_{min} (N·m)	24.68	24.77
ΔT (N·m)	1.25	1.31
TRR (%)	4.95	5.20

5. Asymmetric Rotor Structure

The torque ripple ratios in Figs. 9 and 10 were calculated by simply averaging the instantaneous torques of Type-Rδ_1 and Type-Rδ_2. In this section, an asymmetric rotor structure, in which two different flux barrier geometries of Type-R-1.7 and Type-R+1.6 are adapted in the same lamination, was proposed. Figure 12 shows the proposed asymmetric rotor structure, and SynRM with this asymmetric rotor is called Type-ASR. The torque performances of Type-ASR are calculated by the two-dimensional FEM and compare the results with those in the previous section.

Table 3 presents the characteristics of Type-R-1.7+1.6 and Type-ASR under maximum torque per ampere (MTPA) control. The characteristics of Type-R-1.7+1.6 was calculated simply by averaging the instantaneous torques for each model of Type-R-1.7 and Type-R+1.6. As shown in Table 3, the average torque for Type-ASR is almost equal to that for Type-R-1.7+1.6, and the torque ripple for Type-ASR is larger by 4.8% than that for Type-R-1.7+1.6.

Figure 13 shows the instantaneous torque versus rotor position angle for Type-R-1.7+1.6 and Type-ASR. As shown in

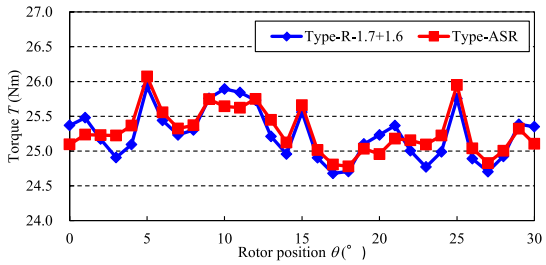

Fig. 13. Instantaneous torque versus rotor position (I_e = 16.4 A, α = 55°)

Fig. 13, the waveforms of the instantaneous torque for each model are slightly different.

6. Combination of Two Different Rotor Laminations in One Rotor

In section 5, an asymmetric rotor structure was used to reduce the torque ripple. In this section, the rotor formed by stacking two different rotor laminations with different flux barrier angle is proposed, and how the torque ripple can be reduced by changing the ratio of stack length of two different rotor laminations is examined. Figure 14 shows the structure of the rotor formed by stacking two different rotors (Rotor A and Rotor B). The stacking method 1 shown in Fig. 14(a) is simple, but the thrust force may be generated. If the thrust force becomes a problem, selecting the stacking method 2 shown in Fig. 14(b) will cancel the thrust force. In the previous section, the combination of Type-R-1.7 and Type-R+1.6 showed the lowest torque ripple. Therefore, our next step was to reduce the torque ripple further by combining Type-R-1.7 (Rotor A) and Type-R+1.6 (Rotor B) as shown.

Figure 15 shows the torque ripple ratio versus the ratio of stack length for Type-R+1.6. The torque ripple ratio is the lowest, at 4.90%, when the stack length ratio of Type-R+1.6 is 45% and the stack length ratio of Type-R-1.7 is 55%. This optimal model is called Type-TDR. Table 2 shows that the ratio of the amplitude of 18th and 36th harmonic components of Type-R+1.6 to Type-R-1.7 is about 55% and 45%. This ratio suggests that the optimal ratio of stack length of Type-R+1.6 to Type-R-1.7 is 45% and 55%, and this result corresponds to Fig. 15.

Table 4 shows the comparison of torque characteristics for Type-R-1.7+1.6 and Type-TDR under MTPA control. Figure 16 shows the instantaneous torque versus rotor position. As shown in Table 4, the average torques for Type-R-1.7+1.6 and Type-TDR are equal and the torque ripple and torque ripple ratio for Type-TDR is slightly lower than that for Type-R-1.7+1.6.

7. Comparison of Reference Model and Optimal Designed Model

In this section, the analysis results for the final designed optimal model (Type-TDR) are compared with those for the reference model (Type-R). Figure 17 shows the instantaneous torque versus rotor position angle for Type-R and Type-TDR, which was obtained by the 2D FEM analysis. As shown in Fig. 17, the average torque for Type-TDR seems almost the same as that for Type-R, but the torque ripple was reduced. Figure 18 shows the amplitudes of the 6th, 18th, and

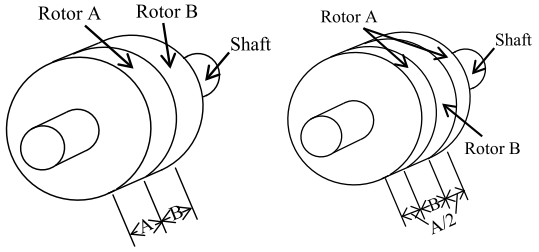

(a) Stacking method 1. (b) Stacking method 2.

Fig. 14. Structure of rotor formed by stacking two different rotors

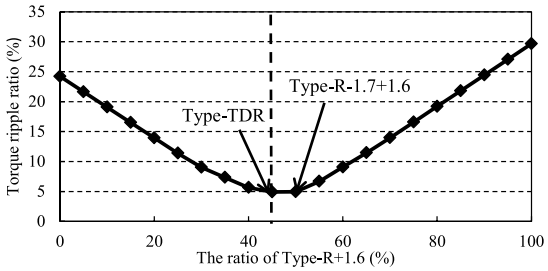

Fig. 15. Torque ripple ratio versus ratio for Type-R+1.6 (I_e = 16.4 A, α = 55°)

Table 4. Torque characteristics under MTPA control (I_e = 16.4 A)

Item (Unit)	Type-R-1.7+1.6	Type-TDR
α (°)	55	55
T_{ave} (N·m)	25.24	25.24
T_{max} (N·m)	25.93	25.99
T_{min} (N·m)	24.68	24.75
ΔT (N·m)	1.25	1.24
TRR (%)	4.95	4.90

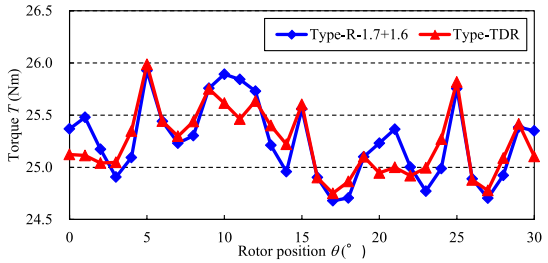

Fig. 16. Instantaneous torque versus rotor position for Type-R-1.7+1.6 and Type-TDR (I_e = 16.4 A, α = 55°)

36th harmonic components of instantaneous torque waveforms for Type-R and Type-TDR. This figure shows that the 18th and 36th harmonic components of instantaneous torque were greatly reduced by using Type-TDR.

Table 5 listed the characteristics for Type-R and Type-TDR calculated by the 2D FEM analysis (2D) and 3D FEM analysis (3D) under MTPA control at the rated speed of 3000 min^{-1}, where the rotor structure of Type-TDR shown in Fig. 14(a) was used for 3D FEM analysis. Comparing the 3D analysis results to the 2D analysis results, the average torque decreased and the torque ripple increased. Although the average torque T_{ave} and efficiency η for Type-TDR are a bit lower than those for Type-R, it can be confirmed that the torque ripple for Type-TDR was reduced to about half

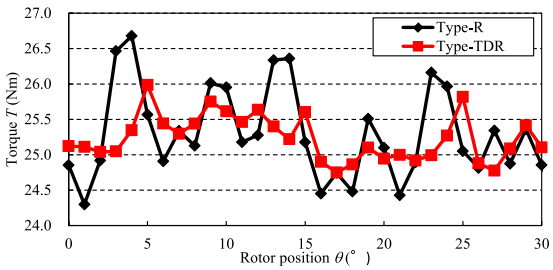

Fig. 17. Torque versus rotor position for Type-R and Type-TDR by the 2D FEM analysis (I_e = 16.4 A, α = 55°)

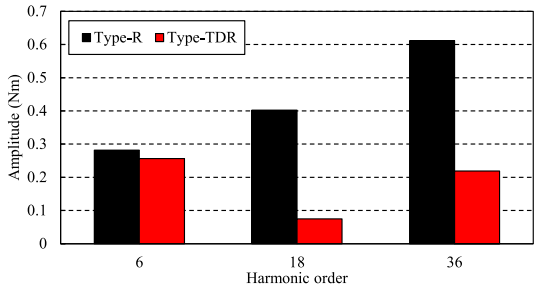

Fig. 18. Amplitude of harmonic components of instantaneous torque waveform for Type-R and Type-TDR (I_e = 16.4 A, α = 55°)

Table 5. Characteristics for Type-R and Type-TDR under MTPA control (I_e = 16.4 A, 3000 min^{-1})

Item (Unit)	Type-R (2D)	Type-R (3D)	Type-TDR (2D)	Type-TDR (3D)
α (°)	55	55	55	55
T_{ave} (N·m)	25.31	24.78	25.24	24.32
ΔT (N·m)	2.41	2.98	1.24	1.44
TRR (%)	9.54	12.02	4.90	5.92
η (%)	94.92	94.36	94.96	94.07

compared to the torque ripple for Type-R in both 2D analysis result and 3D analysis result.

8. Conclusions

This study examined how to reduce the torque ripple in an SynRM without reducing the average torque by combining different flux barrier structure. The analysis results showed that the flux barrier angle influences the torque ripple, and the amplitude and phase of the harmonic components, especially the 18th and 36th harmonic components. Consequently, an asymmetric rotor structure having two flux barrier designs (Type-ASR) in which two different flux barrier geometries of Type-R-1.7 and Type-R+1.6 are adapted in the same lamination was proposed. By combining two different flux barrier structures, which cancelled the 18th and 36th harmonic components for each model, the torque ripple was greatly reduced. The torque ripple was further reduced by adjusting the ratio of stack length of Type-R-1.7 and Type-R+1.6. The average torque for Type-TDR, the proposed model with optimal ratio of stack length, was almost equal to that for the reference model Type-R, and the torque ripple for Type-TDR was greatly reduced, and was about half lower than that for Type-R.

The torque ripple reduction method proposed in this paper utilizes the change of the main harmonic components of the torque ripple due to the shift of the flux barriers, and based on the cancelation of the harmonic components by the combination of the two types of flux barrier structures. It is difficult to theoretically clarify the optimum shift angle of the magnetic flux barrier due to nonlinearity in the magnetic circuit of SynRM, but the design process proposed in this paper is effective for selecting the optimum shift angle and finding the combination of the two kinds of rotor structures in order to reduce the torque ripple.

The effect of reducing the torque ripple was confirmed by the FEM analysis result in this paper. Although the accuracy of torque calculated by the FEM analysis is considered to be sufficiently high, verification by experiment is also important. In the next step we are planning to manufacture a prototype and verify its characteristics by experiments.

References

(1) S. Morimoto, Y. Asano, T. Kosaka, and Y. Enomoto: "Recent Technical Trends in PMSM", 2014 International Power Electronics Conference, pp.1997–2003 (2014)

(2) T. Ota: "Rare Earth Resources and Related Industries in Japan", in Journal of MMIJ, Vol.127, pp.549–557 (2011)

(3) I. Boldea, L.N. Tutelea, L. Parsa, and D. Dorrell: "Automotive Electric Propulsion Systems With Reduced or No Permanent Magnets: An Overview", IEEE Trans. on Industry Electronics, Vol.61, No.10, pp.5696–5711 (2014)

(4) T. Matsuo and T.A. Lipo: "Rotor Design Optimization of Synchronous Reluctance Machine", IEEE Trans. on Energy Conversion, Vol.9, No.2, pp.359–365 (1994)

(5) Y. Honda, S. Kawano, H. Kiriyama, T. Higaki, S. Morimoto, and Y. Takeda: "Rotor Design and Perfoemances of a Multi-Flux Barrier Synchronous Reluctance Motor", IEEJ Trans. Industry Applications, Vol.118, No.10, pp.1177–1184 (1998) (in Japanese)

(6) A. Vagati, M. Chiampi, M. Pastorelli, and M. Repetto: "Design Refinement of Synchronous Reluctance Motors Through Finite-Element Analysis", IEEE Trans. on Industry Applications, Vol.36, No.4, pp.1094–1102 (2000)

(7) M. Kondo: "An Analysis on Synchronous Reluctance Motors by Use of Magnetic Circuit", IEEJ Trans. Industry Applications, Vol.123, No.2, pp.90–95 (2003) (in Japanese)

(8) K. Kim, J.S. Ahn, S.H. Won, J. Hong, and J. Lee: "A Study on the Optimal Design of SynRM for the High Torque and Power Factor", IEEE Trans. on Magnetics, Vol.43, No.6, pp.2543–2545 (2007)

(9) R.R. Moghaddam, F. Magnussen, and C. Sadarangani: "Theoretical and Experimental Reevaluation of Synchronous Reluctance Machine", IEEE Trans. on Industry Electronics, Vol.57, No.1, pp.6–13 (2010)

(10) A.T. de Almeida, F.J.T.E. Ferreira, and G. Baoming: "Beyond Induction Motors-Technology Trends to Move Up Efficiency", IEEE Trans. on Industry Applications, Vol.50, No.3, pp.2103–2114 (2013)

(11) A. Vagati, M. Pastorelli, G. Franceschini, and S.C. Petrache: "Design of Low-Torque-Ripple Synchronous Reluctance Motors", IEEE Trans. on Industry Applications, Vol.34, No.4, pp.758–765 (1998)

(12) M. Sanada, K. Hiramoto, S. Morimoto, and Y. Takeda: "Torque Ripple Improvement for Synchronous Reluctance Motor Using an Asymmetric Flux Barrier Arrangement", IEEE Trans. on Industry Applications, Vol.40, No.4, pp.1076–1082 (2004)

(13) N. Bianchi, S. Bolognani, D. Bon, and M.D. Pré: "Torque Harmonic Compensation in a Synchronous Reluctance Motor", IEEE Trans. on Energy Convention, Vol.23, No.2, pp.466–473 (2008)

(14) N. Bianchi, S. Bolognani, D. Bon, and M.D. Pré: "Rotor Flux-Barrier Design for Torque Ripple Reduction in Synchronous Reluctance and PM-assisted synchronous Reluctance Motors", IEEE Trans. on Industry Applications, Vol.45, No.3, pp.921–928 (2009)

(15) E. Howard, M.J. Kamper, and S. Gerber: "Asymmetric Flux Barrier and Skew Design Optimization of Reluctance Synchronous Machines", IEEE Trans. on Industry Applications, Vol.51, No.5, pp.3751–3760 (2015)

(16) Y. Yamamoto, S. Morimoto, M. Sanada, and Y. Inoue: "Torque Ripple Reduction Using Asymmetric Flux Barriers in Synchronous Reluctance motor", IPEC-Niigata 2018, pp.3197–3202 (2018)

Yuuto Yamamoto (Student Member) received the B.E. degrees from Osaka Prefecture University, Sakai, Japan, in 2016. He is currently a graduate student in the Department of Electrical and Information Systems, Osaka Prefecture University. His research interests include synchronous reluctance machine designs.

Shigeo Morimoto (Senior Member) received the B.E., M.E., and Ph.D. degrees from Osaka Prefecture University, Sakai, Japan, in 1982, 1984, and 1990, respectively. In 1984, he joined Mitsubishi Electric Corporation, Tokyo, Japan. Since 1988, he has been with the Graduate School of Engineering, Osaka Prefecture University, where he is currently a Professor. His main areas of research interest are permanent magnet synchronous machines, reluctance machines and their control systems. Dr. Morimoto is a member of the IEEE, the Society of Instrument and Control Engineers of Japan, the Institute of Systems, Control and Information Engineers, and the Japan Institute of Power Electronics.

Masayuki Sanada (Senior Member) received the B.E., M.E., and Ph.D. degrees from Osaka Prefecture University, Sakai, Japan, in 1989, 1991, and 1994, respectively. Since 1994, he has been with the Graduate School of Engineering, Osaka Prefecture University, where he is currently an Associate Professor. His main areas of research interest are permanent-magnet motors for direct-drive applications, their control systems, and magnetic field analysis. Dr. Sanada is a member of the IEEE, the Japan Institute of Power Electronics, and the Japan Society of Applied Electromagnetics and Mechanics.

Yukinori Inoue (Member) received the B.E., M.E., and Ph.D. degrees from Osaka Prefecture University, Sakai, Japan, in 2005, 2007, and 2010, respectively. Since 2010, he has been with the Graduate School of Engineering, Osaka Prefecture University, where he is currently an Associate Professor. His research interests include control of electrical drives, in particular, the direct torque control of permanent magnet synchronous motors and position sensorless control of these motors. Dr. Inoue is a member of the IEEE and the Japan Institute of Power Electronics.